ELSEVIER

Earth and Planetary Science Letters 189 (2001) 115–131

EPSL

www.elsevier.com/locate/epsl

On the dynamics of the Juan de Fuca plate

Rob Govers *, Paul Th. Meijer

Faculty of Earth Sciences, Utrecht University, P.O. Box 80.021, 3508 TA Utrecht, The Netherlands

Received 11 October 2000; received in revised form 17 April 2001; accepted 27 April 2001

Abstract

The Juan de Fuca plate is currently fragmenting along the Nootka fault zone in the north, while the Gorda region in the south shows no evidence of fragmentation. This difference is surprising, as both the northern and southern regions are young relative to the central Juan de Fuca plate. We develop stress models for the Juan de Fuca plate to understand this pattern of breakup. Another objective of our study follows from our hypothesis that small plates are partially driven by larger neighbor plates. The transform push force has been proposed to be such a dynamic interaction between the small Juan de Fuca plate and the Pacific plate. We aim to establish the relative importance of transform push for Juan de Fuca dynamics. Balancing torques from plate tectonic forces like slab pull, ridge push and various resistive forces, we first derive two groups of force models: models which require transform push across the Mendocino Transform fault and models which do not. Intraplate stress orientations computed on the basis of the force models are all close to identical. Orientations of predicted stresses are in agreement with observations. Stress magnitudes are sensitive to the force model we use, but as we have no stress magnitude observations we have no means of discriminating between force models. Model stresses in the north and the south of the Juan de Fuca plate are similar. Breakup along the Nootka fault zone, and not in the Gorda region, can be explained if the local strength of a lithosphere column depends on lithospheric age. Stresses are invariant to whether or not transform push is acting on the Mendocino Transform fault. We therefore conclude that the introduction of this extra plate driving force is not required by observations for the Juan de Fuca plate.

Keywords: intraplate processes; stress; Cascadia subduction zone; Mendocino fracture zone; Gorda Plate; plate tectonics

1. Introduction

Convergence between the subduction zone off the North American west coast and the East Pacific Rise has resulted in fragmentation of the Farallon plate into smaller plates [1,2]. Since the Oligocene, the Farallon plate has broken into the Cocos, Nazca, and Juan de Fuca plates, and into various microplates. The approach to the various subduction zones of the ridge system continues today and plate fragmentation perseveres. Since about 4 Ma the northernmost end of the Juan de Fuca plate is in the process of slowly breaking away [3] at a rate of approximately 1 mm/yr [4]. Hyndman et al. [3] identified the incipient plate boundary on the basis of seismicity data and seismic reflection data and named it the Nootka fault zone (Fig. 1). It represents the transition from the intraplate deformation zone in the northern sec-

* Corresponding author. Tel.: +31-30-2534-985; Fax: +31-30-2535-030; E-mail: govers@geo.uu.nl

0012-821X/01/$ – see front matter
PII: S0012-821X(01)00360-0

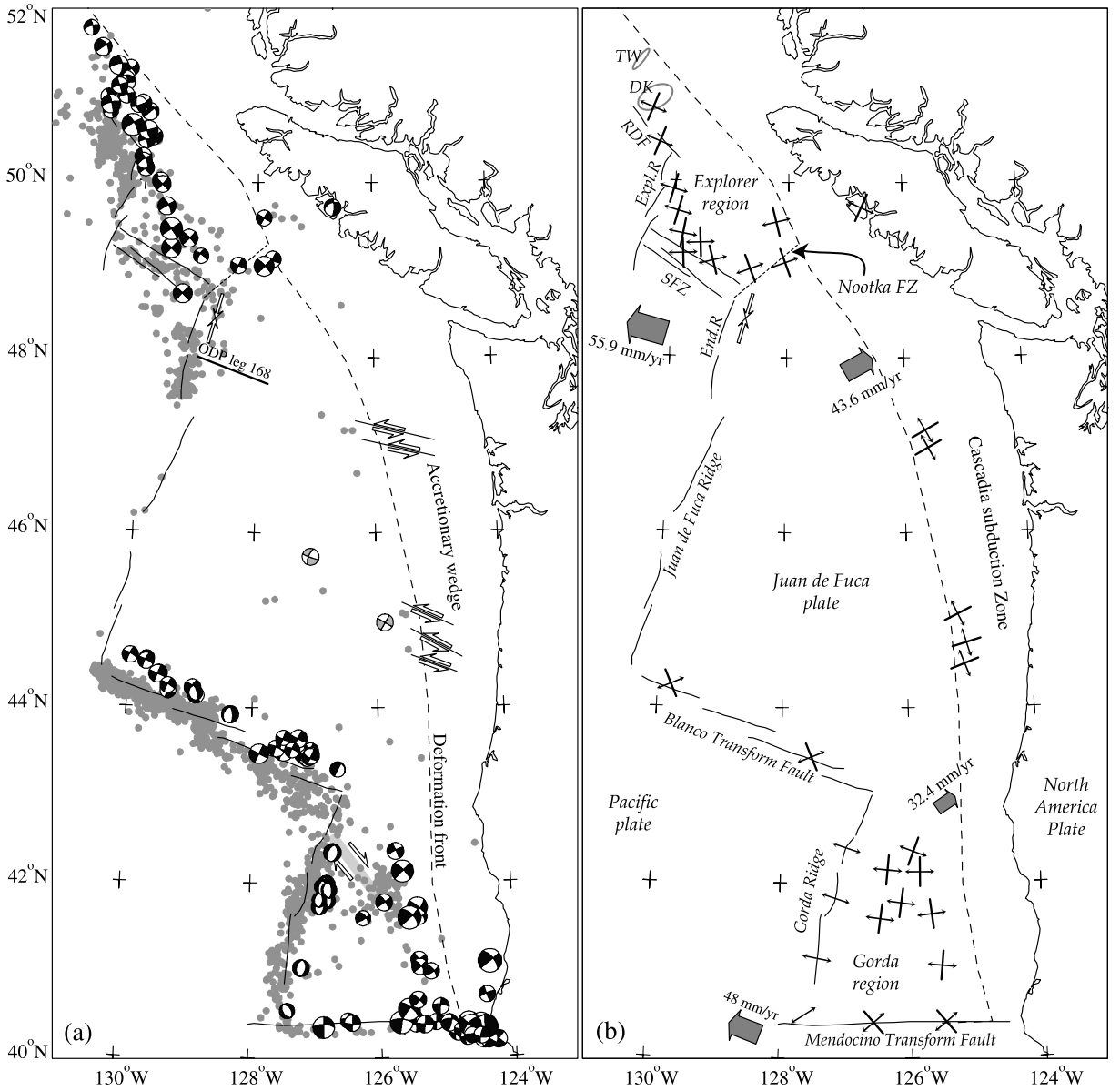

Fig. 1. Major tectonic elements of the Juan de Fuca plate. (a) Stress and strain observations. Focal mechanisms shown in black and white are taken from the CMT catalog (January 1977–May 2000; http://www.seismology.harvard.edu/CMTsearch.html). Focal mechanisms in gray and white are from the study of Spence [8]. Small gray spheres represent epicenters located by the SOSUS hydrophone arrays during 1991–1993 and during 1998 and 1999 ([10]; http://www.pmel.noaa.gov/vents/home.html). Basement cutting faults in the accretionary wedge were identified by Goldfinger et al. [13] from sonar, seismic reflection, and bathymetry data and from submersible observations. The gray shear band in the northwestern Gorda region was identified by Wilson [5] from magnetic anomaly and sonar data. Open arrows at 48.4°N, 128.7°W represent the principal compression obtained from breakouts by A. Krammer as a contribution to the World Stress Map Project [18]. (b) Principal stress directions inferred from observations shown in panel a, relative motion vectors between Juan de Fuca and North America, and between the Pacific plate and the Juan de Fuca plate [4,50]. Abbreviations: DK = Dellwood knolls, End.R. = Endeavour ridge, Expl.R. = Explorer ridge, RDF = Revere–Dellwood fault, SFZ = Sovanco fracture zone, TW = Tuzo Wilson volcanic field.

tion of the Juan de Fuca plate (the Explorer region) to the more rigid central part to the south of it. The southern end of the Juan de Fuca plate, the Gorda region, has also been shown to deform internally, but not to the extent that the plate is fragmenting [5].

Intraplate deformation and plate fragmentation must be caused by forces acting on the Juan de Fuca plate. We therefore develop a consistent force model for the current Juan de Fuca plate in this paper. The force model is based on the inference that magnetic anomaly data require a pole of Juan de Fuca–North America relative motion which has been constant since 0.78 Ma [4]. This shows that the current Juan de Fuca plate did not accelerate or decelerate and, therefore, is mechanically balanced. A principal advantage of this approach is that the constraint of zero net torque can be used to determine forces which are not a priori known. The resulting force model will be used to compute intraplate stresses and strain rates which will be compared with observations. We aim to better understand why the Juan de Fuca plate is fragmenting, why this is happening along the Nootka fault zone, and why the Gorda region is not breaking away.

Previous work addressing the cause of breakup of the Farallon plate into the Cocos and Nazca plates was done by Wortel and Cloetingh [6]. They concluded that strong variations in the age of the slab at the trench can lead to 500–600 MPa stresses within the plate. The authors suggested that such stress levels are high enough to break the plate. Wortel and Cloetingh [6] pictured the same mechanism to have been responsible for fragmentation of other oceanic plates. Whether variations in plate ages at the Cascadia subduction zone suffice to explain breakup of the Juan de Fuca plate is, however, unclear.

The Juan de Fuca plate is small relative to the plates surrounding it. Large plates are mostly driven by body forces within the plate itself. Microplates are slaves to the large plates which surround them, i.e. we expect microplates to be driven by their neighbors. The Juan de Fuca plate is not a microplate, but potentially some fraction of the forces driving it may derive from the Pacific or North America plates. Normal stresses across transform faults have been proposed to transfer an external driving force to the Juan de Fuca plate. This force was called transform push by Wang et al. [7]. Through the torque balance approach we adopt, we aim to establish the possible significance of transform push for Juan de Fuca dynamics.

Previous studies of the dynamics of the Juan de Fuca plate focused either on the Juan de Fuca plate plus part of the North America plate [8], or on parts of the Juan de Fuca plate [7,9]. As neither of these studies started working from the scale of the entire mechanical units on the Earth's surface, the plates, they could not use torque balance of those plates to produce consistent force boundary conditions.

2. Observations

Various observations document that the Explorer and Gorda regions of the Juan de Fuca plate are deforming. Fig. 1a shows the various data which are indicative of Juan de Fuca stresses, Fig. 1b shows our interpretation of these data which is used to judge the quality of the stress models we develop.

Fig. 1a displays intraplate and plate boundary seismicity. Seismic activity is notably absent along the Juan de Fuca ridge, except for the northernmost (Endeavour) segment, and along the eastern subduction plate boundary. Intraplate seismicity concentrates in the Gorda and Explorer regions. Gray circles represent epicenters from the VENTS data collection program of NOAA (http://www.pmel.noaa.gov/vents/home.html) during the periods 1991–1993 and 1998–1999. Events are recorded by the SOSUS hydrophone arrays which provide omni-directional coverage of acoustic rays entering through the ocean bottom and traveling through the water layer [10]. Shallow offshore events can therefore be located more accurately by SOSUS hydrophones than by land-based seismometers, which suffer from one-sided directivity of ray paths, especially for smaller events. This is particularly clear in Fig. 1a; hydrophone-based epicenters occur symmetrically around bathymetric features which have been

identified as plate boundaries, whereas CMT epicenters occur landward from the plate boundaries. Our interpretation of available stress data in Fig. 1b therefore shows *P*- and *T*-axes from the CMT solutions at epicenter locations identified by SOSUS, i.e. shifted to the west by up to 60 km. This is consistent with the shift which was needed for earthquakes in the Explorer region on the basis of ocean bottom seismometer data [11]. Principal stress directions may deviate from *P*- and *T*-axes by ±45° [12].

From basement bathymetry in the Gorda region Wilson [5] identified fault scarps formed at the ridge axis. Together with magnetic anomaly data, these data are shown to be consistent with a distributed zone of right lateral shear deformation (schematically indicated in Fig. 1a). This result is consistent with regional *P*- and *T*-axes. Principal stress directions (Fig. 1b) derived from the orientation of this shear zone suffer from the same ±45° uncertainty as those derived from focal mechanisms.

Goldfinger et al. [13] investigated the central Cascadia submarine forearc using sonar, seismic reflection, and bathymetry data and submersible observations. They identified left lateral faults in the accretionary wedge, some of which also cut into the Juan de Fuca basement (Fig. 1a). Goldfinger et al. [13] note that the focal mechanism obtained by Spence [8] (shown in white and gray in Fig. 1a) is inconsistent with their observations, so that there are two possibilities: either the faults are old and no longer active or the epicenter is not correctly located. The first option is unlikely because seismic sections reveal that the faults cut the sediment–ocean interface. Therefore, we conclude that the epicenter has been incorrectly located and should probably be placed further outboard. The other central Juan de Fuca event studied by Spence [8] probably suffers from the same problem. As we do not know how far out the events should be re-located, we decided not to use their *P*- and *T*-axes.

Various Ocean Drilling Program (ODP) cruises have investigated the Juan de Fuca plate. Leg 139 focused on the northern end of the Juan de Fuca ridge system near its intersection with the Sovanco fault zone [14]. Based on seismic reflection data, heat flow measurements, and bathymetry data, Davis and Villinger [15] conclude that here the rift is 'starved'. ODP Leg 168 (Fig. 1a) established that no recent deformation took place along the profile [16], consistent with the findings of Rohr [17].

A principal compression direction was established from breakouts by Anton Krammer as a contribution to the World Stress Map Project [18]. The database specifies no standard deviation for this particular direction, but based on the B-quality assigned to this observation in the database, its standard deviation should be less than or equal to ±20°.

In most of the Juan de Fuca plate, the intermediate principal stress axis is oriented vertically (Fig. 1b). Maximum compression and tension directions are horizontal, and the overall stress regime therefore is strike-slip. Near the Cascadia subduction zone, maximum tension axes are oriented NNW–SSE. Further outboard, principal tension directions are close to E–W.

3. Force model

3.1. General approach

Historically, force models were developed first for the larger plates: the Nazca plate [19,6], the Indo-Australia plate [20,21], the North America plate [22], the Pacific plate [23], the South America plate [24–27], and the African plate [28,29]. Plate driving forces like ridge push and slab pull can be reasonably well estimated but magnitudes of the remaining forces are unknown and have to be solved by mechanically balancing the plate [30]. Observations of stress directions have successfully been reproduced for the larger plates. For the Indo-Australian and Pacific plates, intraplate stress magnitudes were estimated from hypocentral depths and were also shown to be consistent with model predictions [23,31]. The torque balance approach works well for the larger plates, i.e. stress fields in the larger plates can be explained by balancing body forces that drive the plate with boundary resistive forces. On the scale of larger plates, approximations in the calculation

of ridge push and slab pull forces are justified. It is a natural progression to start focusing on smaller lithosphere plates and to more accurately estimate driving body forces. Also, it is to be expected that smaller plates are driven to a lesser extent by internally generated forces and more by surrounding plates.

3.2. Model geometry and plate boundaries

The Juan de Fuca plate is a relatively small oceanic plate between the Pacific and North America plates. Half spreading rates on its western plate boundaries are of the order of 25–35 mm/yr so that, by the time Juan de Fuca plate material reaches the Cascadia subduction plate boundary, the plate is maximally 11 Myr old. Fig. 2 shows the geometry of the model Juan de Fuca plate, the crustal age distribution, and the interpretation of plate boundary types we use. At the scale of the whole plate, crustal ages are well constrained [4]. Points of uncertainty in defining the model geometry are where to put the Cascadia plate boundary and the shape of the Explorer region.

The introduction of a subduction boundary in our mechanical model is artificial in the sense that the surface Juan de Fuca plate is continuous with the subducted Juan de Fuca plate. In our mechanical model, slab pull forces and forces resisting subduction and relative motion between the Cascadia slab and the North America plate will be assumed to act at the eastern boundary. If chosen correctly, these boundary conditions mimic the dynamic influence of plate forces beyond the model's eastern boundary. This model boundary is optimally chosen as far east as possible, which is the line where plate contact forces start becoming relevant. Mechanically, the accretionary wedge will be of little influence on the dynamics of the Juan de Fuca plate. This is evident from the high degree of deformation of the wedge relative to the underlying Juan de Fuca plate (figure 2 of [13]). We therefore select the model plate boundary east of the wedge deformation front. The model subduction boundary was digitized from a bathymetric map of the continental margin of western Canada [32] by approximately tracking the shelf edge. Offshore Oregon and southern Washington this coincides roughly with the location of the Siletz(ia) terrane which was identified by Trehu et al. [33] as the mechanical backstop for accretionary wedge deformation.

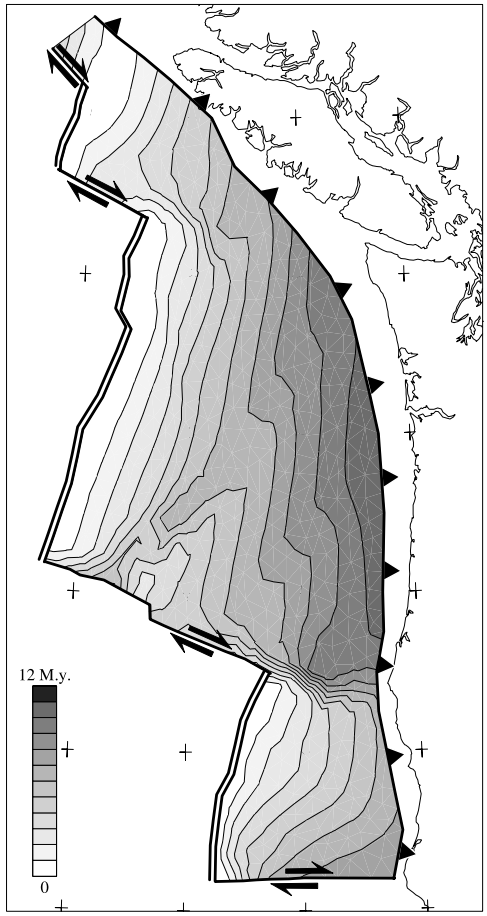

Fig. 2. Plate boundary types and age distribution adopted in this study [4]. Double lines represent ridge boundaries. The barbed line is a subduction boundary with solid triangles pointing to the overriding plate. Transform boundaries are labeled with arrows to show their sense of relative motion.

The nature of plate boundaries surrounding the Explorer region has been subject to debate. Riddihough and Hyndman [34] argued that the Explorer region is bounded by the Sovanco fracture zone, Explorer ridge, Revere–Dellwood fault, a ridge system crossing Tuzo Wilson volcanic field and Dellwood knolls, and an eastern plate boundary where the Explorer subducts under North

America. On the basis of bathymetry and seismicity data, Rohr and Furlong [35] put forward the view that the Explorer ridge is a failing plate boundary, that Tuzo Wilson volcanic field and Dellwood knolls do not constitute a ridge system and that subduction of the Explorer region beneath North America never occurred. Instead, they proposed a transform plate boundary which dissects the Explorer region along the main trend of the seismicity [36]. Implicit in this scenario is that the Nootka fault zone is evolving to become the plate boundary between the North America plate and the Juan de Fuca plate. Seismic reflection [36], bathymetry [3,15], and gravity [3] data consistently indicate that the the amount of slip across the Nootka fault zone is limited and, therefore, that this evolution has not progressed very far. In our modeling, we deal with these uncertainties by assuming the plate boundary geometry as proposed by Riddihough and Hyndman [34], and investigate the sensitivity of our model results by assuming either a subduction or a collision plate boundary at the Explorer–North America interface.

The Sovanco fracture zone is not a well-developed transform fault, but a 15 km wide region of distributed right lateral faulting [37]. At the scale of our model the Sovanco fracture zone can, however, be approximated as a transform fault.

3.3. Model forces

3.3.1. Ridge push

The first major driving force that acts on the Juan de Fuca plate is ridge push (F_{rp}). Contrary to what the name suggests, ridge push is not a boundary force acting at the ridge axis but a horizontal pressure gradient integrated over the area of the plate [38]. This pressure gradient results from cooling, densification and isostatic sinking of the oceanic lithosphere. Following Meijer and Wortel [29], ridge push is calculated from crustal age using thermal model GDH1 [39]. Lithospheric ages for the Juan de Fuca stress model are taken from the digital age grid of Müller et al. [40]. Ridge push is typically computed from age gradients which follow from finite rotation poles. However, ridge propagators have been prominent features in the development of the Juan de Fuca plate. As the stage pole approach does not account for ridge propagators, we use horizontal age gradients computed directly from the age grid data to calculate ridge push forces. The results are identical in regions where the spreading history is simple and ridge propagators are absent, but can locally deviate substantially from the results obtained by projection.

3.3.2. Slab pull

The second driving force is slab pull (F_{sp}), which is the down-dip component of the gravity body force that acts on the dense slab. Slab pull acts on the model subduction boundary. We compute the slab pull force by integrating density anomalies from the trench up to the end of the slab. Density anomalies are calculated from a thermal model in which the slab had a GDH1 geotherm at the trench, and which is conductively heated after the slab has sunk beneath the overriding plate. The most relevant difference with previous methods of calculating the slab pull force (a detailed account is given by Wortel et al. [23]) is that we integrate density differences up to the tomographically 'observed' slab length. In previous studies, integration was taken up to the maximum depth of seismicity, which was predicted from the oceanic age at the trench and the convergence velocity [23]. The maximum seismic depth is predicted to be 50 km for the Cascadia slab, whereas tomographic results indicate a slab of the order of a few hundred km [41,42]. This results in 1.7–2.5 times higher slab pull forces for the Juan de Fuca plate.

The average slab dip is reasonably well constrained by tomographic results to be in the range 45–65°. In our study, we therefore adopt a slab dip of 54°; slab dips of 45° and 65° are equivalent with 10% lower and 10% higher values of the slab pull force. The slab end is less easily resolved from tomographic studies due to downward streaking. Best estimates range between 200 and 400 km depth ([41,42]; W. Spakman, personal communication, 2000). The slab pull torque for a 400 km deep slab is 1.5× larger than the torque for a slab penetrating to 200 km depth. These differences are potentially important, which is

why we will compare models for a 200 km deep slab with models with a slab end at 400 km depth.

3.3.3. Transform push

The introduction of this third driving force acting on the Juan de Fuca plate was proposed by Wilson [43] and Richardson and Reding [22]. Physically, transform push is a boundary force resulting from normal stresses that are transmitted across strike slip faults. The argument against significant normal stress has been based on the inference that shear stresses at strike slip faults are low, for instance from stress orientation and heat flow measurements. The key to this argument is that for brittle faults it has been established that the shear stress is proportional to the normal stress. The proportionality constant is, however, not well established for plate boundaries. Moreover, transform plate boundaries extend down into the ductile creep regime, making an assessment of the relation between shear and normal stresses even more difficult. Therefore, observations of low shear stresses do not necessarily demonstrate low normal stresses in our opinion.

In our model, we parameterize transform push (F_{tp}) as being proportional to the relative velocity perpendicular to transform segments of the Juan de Fuca plate. The Pacific plate has a significant component of relative motion normal to the Mendocino fault. On the other transform faults, Pacific normal motion is negligible. Transform push therefore acts on the model Mendocino fault only.

3.3.4. Transform fault shear resistance

The transform fault resistive force (F_{tf}) to strike slip motion is assumed to result from a uniform value of the shear stress at transform plate boundaries in our model. We use this parameterization because it is the most simple one. Transform faults resistance acts on all model transform faults.

3.3.5. Basal drag

Basal drag is the integrated shear traction acting on the base of a plate due to the relative motion between the plate and the mantle. How convective flow beneath the plates relates to plate motions is unclear. Even the question of whether mantle convection is resistive or driving in plate motions is uncertain. Plate dynamic modeling studies on other plates have solved the magnitude of the basal drag torque in the direction of absolute plate motion. It was concluded that the basal shear stress magnitude that can be derived from the basal drag torque is of the order of a few MPa only. Most of the studied plates are concluded to experience a net resistance by mantle flow. The South America plate may be an exception to this [27]. One of the consequences of the relatively small size of the Juan de Fuca plate is that the basal drag torque is small. For most of our models we select a resistive basal shear stress of 0.1 MPa that acts uniformly along the base of the Juan de Fuca plate in the direction of absolute plate motion ('hotspot reference frame', [4]).

3.3.6. Subduction resistive forces

Three resistive forces act on the slab at the subduction plate contact and in the upper mantle: (1) compositional buoyancy (F_{cb}), which is the gravity body force of shallow oceanic crust and mantle which is buoyant relative to the upper mantle; (2) plate contact shear force (F_{pc}), the shear stress between the subducting and the overriding plate integrated along the contact region; (3) slab resistance force (F_{sr}), the force resulting from integration of the mantle shear stress acting on the top and bottom of the slab. F_{cb} and F_{sr} act in the up-dip direction of the subducted slab, and F_{pc} acts in the direction of relative plate motion. These are rather typical parameterizations. These subduction resistive forces act as boundary conditions on the subduction model boundary. The plate contact resistance has both trench-parallel and trench-normal components because the Juan de Fuca plate subducts obliquely beneath North America. Our parameterization of the plate contact resistance is more simple than that of Wang et al. [7], who separately solved the parallel and normal components of the plate contact resistance, thereby effectively making the resistance anisotropic.

3.3.7. Collision force

As discussed in Section 3.2, the uncertain nature of the eastern plate boundary of the Explorer

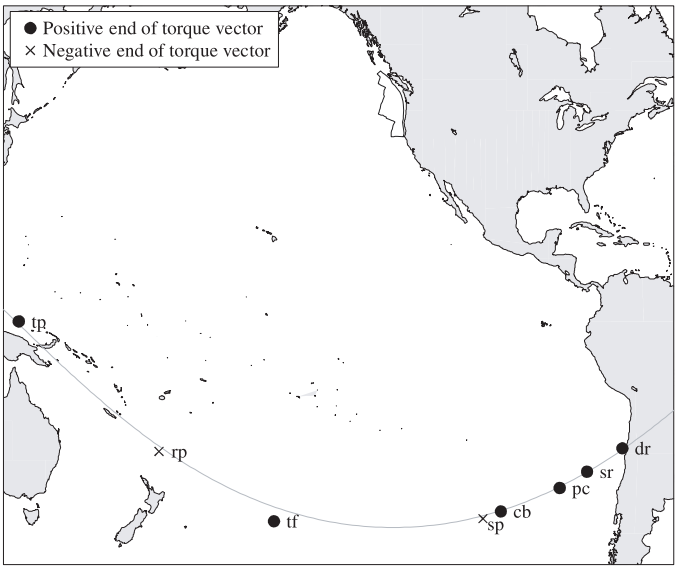

Fig. 3. Intersections of torque vectors and the Earth's surface. The gray line represents the great circle around the approximate Juan de Fuca plate center (46°N, 127°W).

region requires us to also consider the possibility that this is a collision boundary. In these alternative models, the collision force F_c acts at the eastern model boundary in the direction of Juan de Fuca–North America relative motion.

3.4. Torque balance results

Mechanical equilibrium follows from a vanishing sum of torques with respect to the center of the Earth:

$$\sum_i \mathbf{T}_i = \sum_i \int_O \mathbf{R} \times \mathbf{F}_i \mathrm{d}O = 0 \qquad (1)$$

where the sum is over all torque vectors $\mathbf{T}_i$ (i = rp, sp, tp, dr, cb, pc, sr), and integration is taken along the boundary O where a particular force type $\mathbf{F}_i$ acts. $\mathbf{R}$ is the radius vector from the center of the Earth to the surface location where a force acts on the Juan de Fuca plate.

Fig. 3 shows the intersections of torque vectors and the Earth's surface for the adopted plate geometry and forces. Also shown is a great circle around 46°N, 127°W, which is the approximate Juan de Fuca plate center. The sign convention is that a torque is positive when it acts to rotate the plate in a counterclockwise direction. It shows that torque vectors lie close to, but not exactly on a single plane implying that the mechanical balance problem is close to being two-dimensional.

Table 1
Torque data

	T_x (Nm)	T_y (Nm)	T_z (Nm)
Transform push			
T_{rp}	1.017×10^{24}	-5.186×10^{22}	5.768×10^{23}
T_{dr}	-5.461×10^{22}	1.708×10^{23}	9.898×10^{26}
T_{tf}	-5.134×10^{24}	-2.346×10^{24}	-5.250×10^{24}
T_{cb}	-3.597×10^{24}	-1.803×10^{25}	-1.608×10^{26}
T_{sp}	7.843×10^{24}	2.817×10^{25}	2.676×10^{26}
T_{sr}	1.480×10^{24}	-9.058×10^{24}	-6.108×10^{24}
T_{tp}	-1.554×10^{24}	1.144×10^{24}	3.575×10^{21}
No transform push			
T_{rp}	1.017×10^{24}	-5.186×10^{22}	5.768×10^{23}
T_{dr}	-5.461×10^{22}	1.708×10^{23}	9.898×10^{22}
T_{tf}	-4.408×10^{24}	-2.014×10^{24}	-4.507×10^{24}
T_{cb}	-4.778×10^{24}	-2.395×10^{25}	-2.136×10^{25}
T_{sp}	7.843×10^{24}	2.817×10^{25}	2.676×10^{25}
T_{sr}	3.805×10^{23}	-2.329×10^{24}	-1.571×10^{24}

Torque vectors in a cartesian frame with x = 0°E, y = 90°E, and z = 0°N for the transform push and no transform push models. Slab pull is computed based on the assumption that the slab penetrates to 300 km depth. Basal shear resistance is 0.1 MPa.

The cause of this is that the Juan de Fuca plate is small. Stable two- and three-dimensional solutions of Eq. 1 were computed and the results differ substantially, indicating that the problem should be treated as three-dimensional. We verified that variations in the adopted plate geometry do not affect this conclusion.

Another observation in Fig. 3 is that torques of the plate contact resistance, deep slab resistance and basal drag lie fairly close together. This is a consequence of the fact that the absolute motion of the Juan de Fuca plate and the North America–Juan de Fuca relative motion are in similar directions. To reduce the number of unknowns in Eq. 1 to three, we assume (a range of) values for torque magnitudes $|\mathbf{T}_{dr}|$ and $|\mathbf{T}_{pc}|$ from previous studies, and solve $|\mathbf{T}_{tp}|$, $|\mathbf{T}_{tf}|$ and a combined torque magnitude $|\mathbf{T}_{sr+pcr}|$. We verified that it did not matter whether the direction of this combined torque vector was taken in the direction of $\mathbf{T}_{pc}$ or $\mathbf{T}_{sr}$.

Fig. 4 summarizes the results of solving Eq. 1 for various assumptions on the compositional buoyancy force F_{cb}, slab penetration depth (Fig. 4a), and basal shear stress (Fig. 4b). We assume that the compositional buoyancy force F_{cb} can lie in the range $3–6\times10^{12}$ Nm^{-1}. The lower value is based on the work of van den Beukel [44]. The upper value was estimated by England and Wortel [45] for the (probably unrealistic) case that the oceanic crust and depleted mantle do not decouple from the rest of the slab at 100 km depth. We only show mechanically feasible results; F_{tp} should be positive to be a driving force, or be zero, $F_{sr}+F_{pc}$ and F_{tf} should be negative to be resistive. Solid lines in the figure are results for a slab penetration depth of 300 km and a 0.1 MPa basal drag.

Fig. 4 shows that there exists a suite of force models which do not require transform push ($T_{tp}=0$). We will refer to these models as 'no transform push' models. These types of models require $F_{sr}+F_{pc}$ to be less resistive than models which do require transform push to establish me-

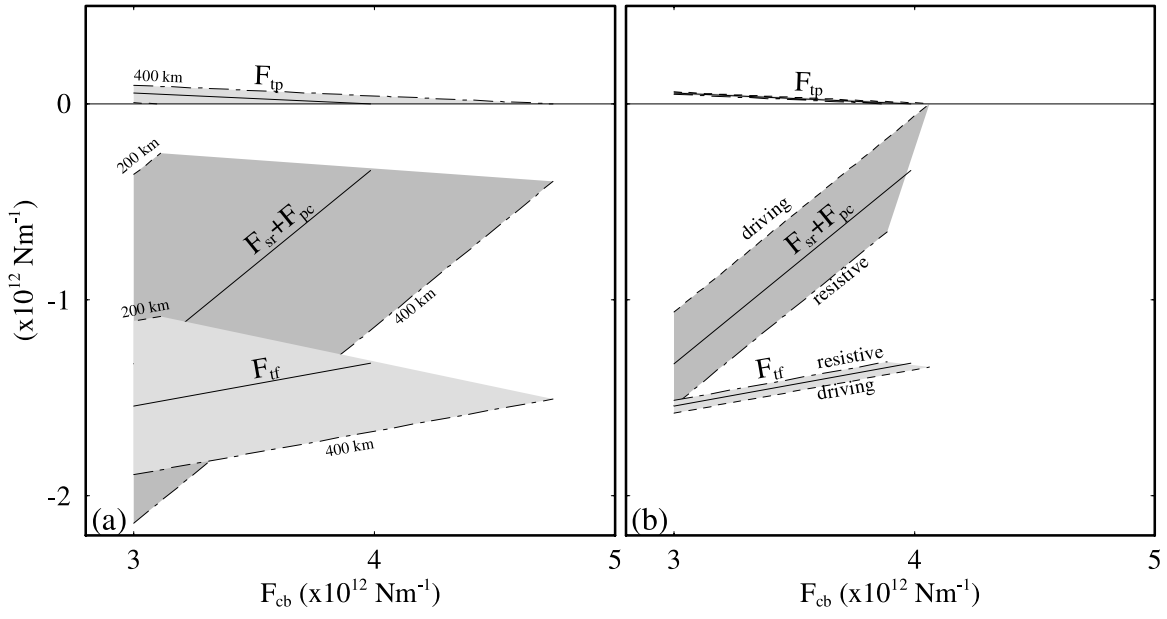

Fig. 4. Torque balance results. Magnitudes of transform push F_{tp}, deep resistance F_{sr} plus plate contact resistance F_{pc}, and transform fault shear resistance F_{tf} as a function of compositional buoyancy. Only the dynamically admissible results are shown, i.e. we do not show results for which shear resistance acts as a driving force, or for which transform push exerts a net pull on the Juan de Fuca plate. (a) Gray areas indicate the sensitivity to the assumed slab length for a resistive basal drag of 0.1 MPa. (b) Sensitivity to variations in basal drag from a 1 MPa resistive basal shear stress to 1 MPa driving basal shear, assuming a slab length of 300 km.

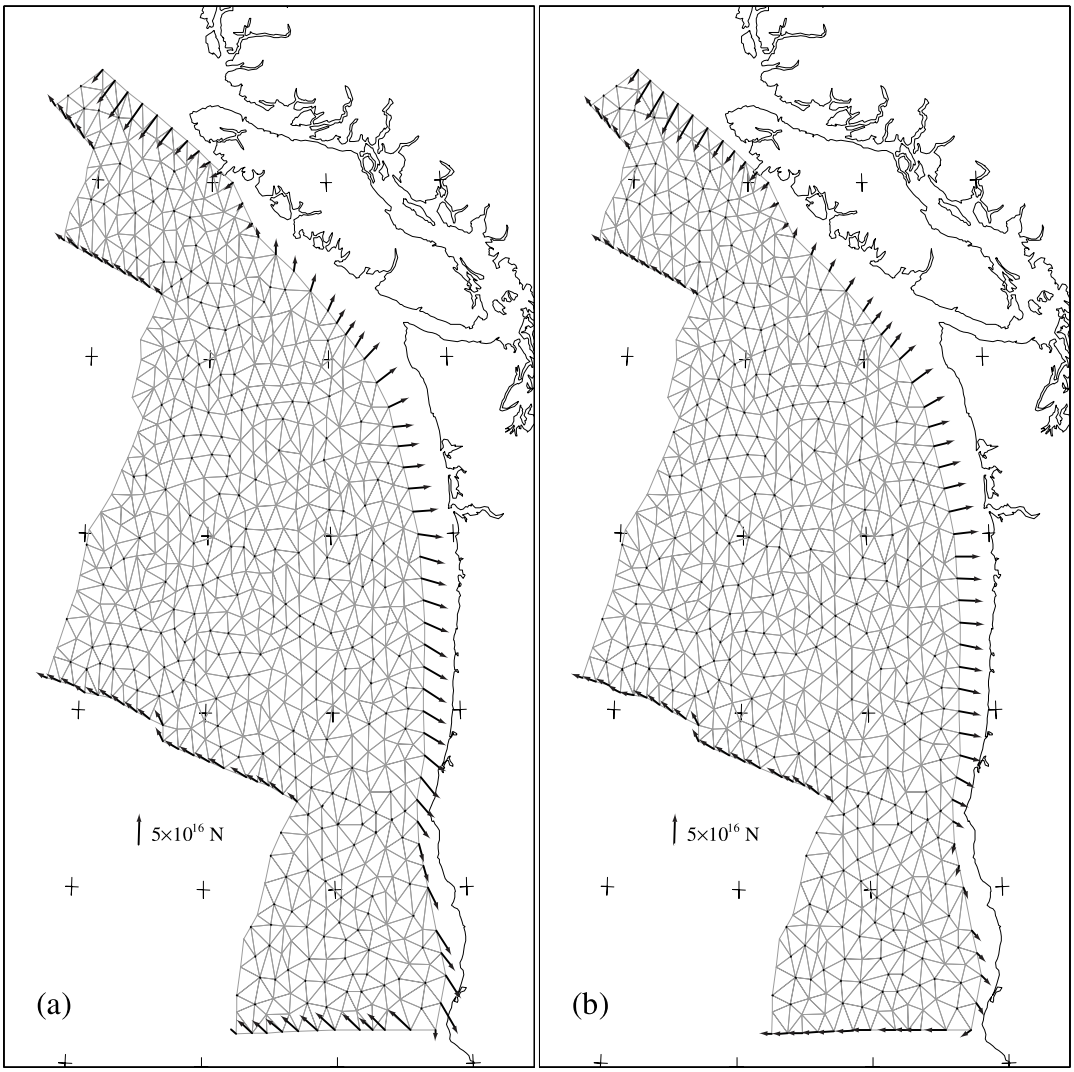

Fig. 5. Node forces and numerical grid. (a) For the transform push model. (b) For the no transform push model.

chanical balance. The end-member suite of models at $F_{cb} = 3 \times 10^{12}$ Nm^{-1} will be referred to as 'transform push' models. Table 1 lists torque vectors for both types of force models. Typical values for the transform fault (shear) resistance found in other plate dynamic studies range from 0.1 to 2×10^{12} Nm^{-1}. Our results fall well within this range. The sum of F_{sr} and F_{pc} was found by Wortel and Cloetingh [46] to be of the order of 3×10^{12} Nm^{-1}. We find lower values, consistent with the fact that the Cascadia slab is shorter than the Nazca slab. We find transform push forces ranging from zero to 1×10^{11} Nm^{-1}, which amounts to an average normal stress of 7 MPa across the Mendocino Transform fault if we assume that the Gorda plate is 50 km thick here.

Torque magnitudes are sensitive to the assumed slab penetration depth, i.e. to the total slab pull torque. Our results show that the sensitivity to the assumed basal shear stress, whether driving or resistive, is not large.

An alternative set of balanced force models follow in case the eastern Explorer plate boundary is a collision rather than a subduction boundary.

Collision is mechanically more difficult than subduction; firstly because there are no slab pull forces acting, and secondly, because there is no subduction fault which facilitates convergence at relatively low shear stresses. Subduction F_{pc} is typically of the order of one or a few 10^{12} Nm^{-1}. Therefore, we a priori constrain the collision force magnitude to be 1×10^{12} Nm^{-1} or higher. We find dynamically admissible force models both with and without transform push. Maximum collision forces range from 1 to 2.7×10^{11} Nm^{-1} for assumed slab penetration depths of 200–400 km, respectively. Diagrams very similar to Fig. 4 (not shown here) follow for this range of collision forces.

4. Stress model

4.1. General aspects

In Section 3, we derived various force models, notably the no transform push and transform push models. We solve the mechanical equilibrium equations

$$\nabla\cdot\sigma = \mathbf{0} \tag{2}$$

in an elastic spherical shell which is subject to the forces we obtained from balancing the torques. This allows us to compute intraplate stresses σ. We modified finite element code TECTON [47] to solve Eq. 2 in a spherical shell geometry using a plane stress approximation. We use a large deformation formalism to guarantee a stress field which is consistent with the force boundary conditions. Regional stresses are computed using a uniform elastic plate with a Young's modulus of 7×10^{10} Pa, and Poisson's ratio of 0.25. Fig. 5 displays the finite element grid we adopt, and the nodal forces for the transform push model and the no transform push model in case the slab is assumed to penetrate to a depth of 300 km and the basal shear resistance is 0.1 MPa.

4.2. Stress field of the Juan de Fuca plate

We computed stress solutions for the spectrum of force models summarized in Fig. 4. In terms of principal stress directions, the resulting stress models vary only in their details, i.e. the general stress direction pattern is largely independent of assumptions on slab length or basal drag. These assumptions do affect stress magnitudes. Regional stresses resulting from the transform push and no transform push force models for a slab penetrating to 300 km depth and a 0.1 MPa basal drag are shown in Fig. 6. Both stress models show plate boundary-parallel tension along the Juan de Fuca–North America margin and ridge-parallel compression in the western part of the Juan de Fuca plate. Tensional and compressional regions are separated by a neutral (low stress) zone. This stress pattern is largely a result of the age variation at the Cascadia trench (Fig. 2). The subducted slab exerts a net pull on the (surface) Juan de Fuca plate north of the Gorda region and south of the Explorer region (cf. Fig. 5). Young lithospheric ages in the Explorer region cause slab pull forces to be smaller than resistive forces in both models. Forces on the Gorda region in both the transform push and the no transform push models act to rotate the Juan de Fuca plate in an counterclockwise sense, which has the same mechanical effect as a net resistance to shear at the eastern plate boundary (Fig. 6, inset). Model stresses reflect the resulting in-plate bending of the surface plate.

Stress magnitudes are 28% higher or lower than shown in Fig. 5 for a slab penetrating up to 400 km and 200 km, respectively. Assuming a basal shear resistance of 1 MPa increases stress magnitudes by 5%. A driving basal shear stress of 1 MPa decreases stress magnitudes by 6%.

Before we compare model stresses with observations it is important to realize that observed stress directions in the Juan de Fuca plate are mostly derived from focal mechanisms and fault slip data. These observations are indicative of the directions of maximum and minimum principal stress. Fig. 7a therefore shows these principal stress directions from the transform push model (Fig. 6a). Intermediate principal stress directions are not shown in the figure. Taking the results from the no transform push model (Fig. 6b) gives identical results. Gray arrows represent the stress

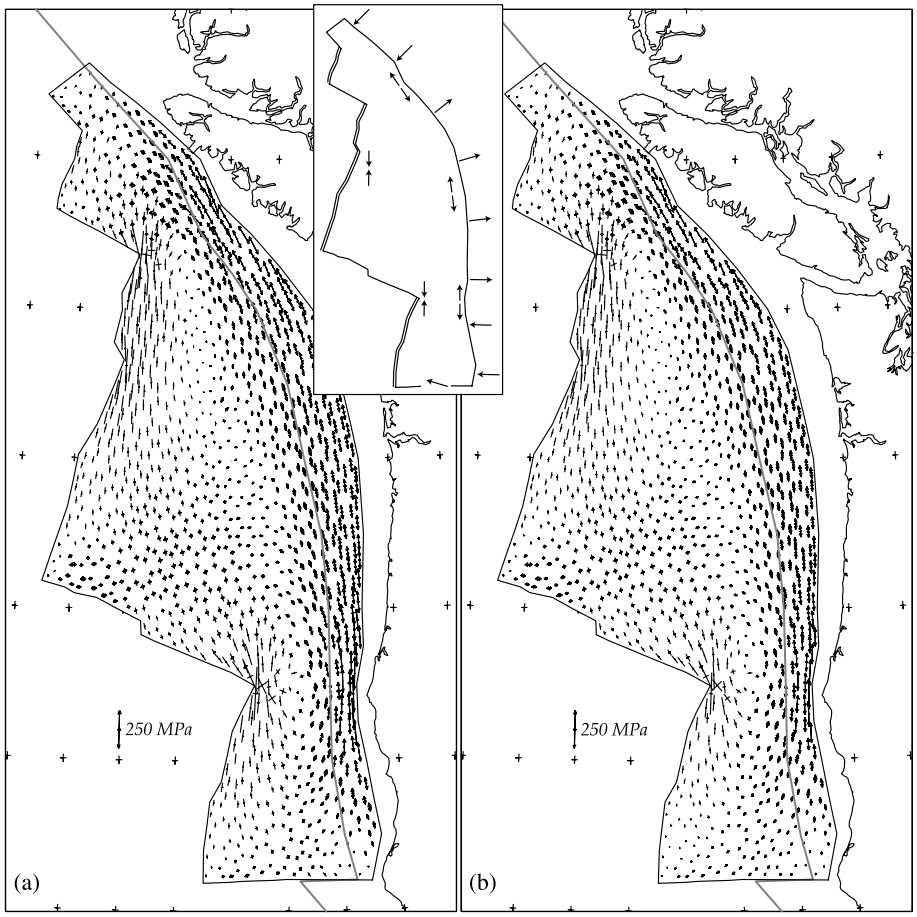

Fig. 6. Juan de Fuca principal stresses. Arrows indicate tensional stress, lines without arrows indicate compression. The gray line shows the accretionary wedge deformation front. (a) Results of the transform push model. (b) Results of the no transform push model. The inset schematically shows how the combination of a net pull along the center of the eastern model margin and net resistance along the Explorer and Gorda regions causes in-plane bending stresses.

'data' from Fig. 1b. Bearing in mind the 45° uncertainty in the stress observations, the fit with model stresses is acceptable. In the Gorda and Explorer regions, model stresses and observations agree to within the data uncertainty. The modeled strike-slip regime near the Blanco Transform is consistent with observations. The model predicts N–S compression near the Endeavour ridge, where bore hole breakouts yield a maximum horizontal compression oriented N19°E. As discussed in Section 2, the model compression direction is therefore within one standard deviation of the observed direction.

The downside of a display of the type shown in Fig. 7a is that the model outcome may appear inconsistent with observations in cases where the magnitude of the intermediate principal stress is very close or equal to either the minimum or maximum principal stress. Model stresses beneath the accretionary wedge suggest a trench-parallel tensile regime, where fault slip observations indicate strike-slip. As the model is based on a plane stress approximation, it can be directly be seen in Fig. 6a that intermediate and minimum eigenvalues in this region are nearly equal, i.e. $\sigma_2 \approx \sigma_3$. Whether the minimum principal stress is oriented vertically or in a direction perpendicular to the trench therefore is not a feature of the model we confidently

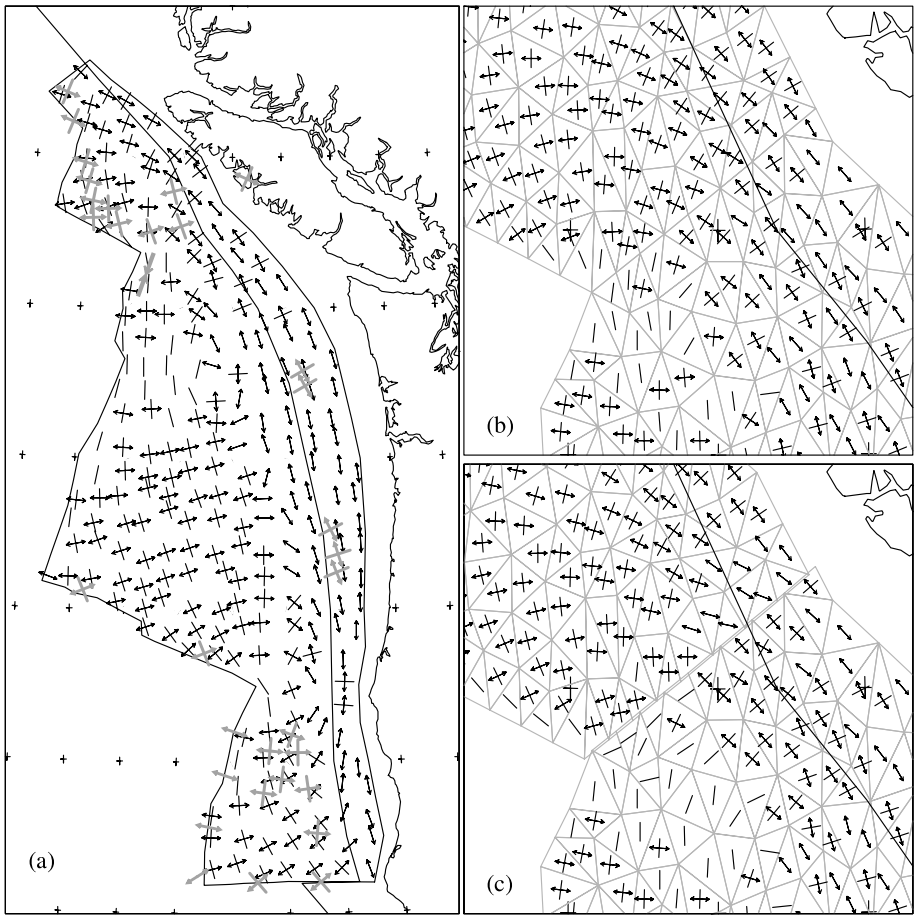

Fig. 7. Directions of maximum and minimum deviatoric stresses in the transform push model. (a) Gray symbols are stress directions taken from Fig. 1b. The gray line represents the accretionary wedge deformation front. (b) Detail of the stress model in panel a in the vicinity of the Nootka fault zone. Gray triangles are the numerical grid. (c) Results of a separate calculation where everything is identical to panels a and b, except that frictional slip is possible along a pre-defined model Nootka fault. The resulting fault offset is most clearly visible as a jump in the boundary of the numerical grid. By comparing panels b and c it is clear that only in the region immediately surrounding the model fault stress orientations change by a small amount.

resolve. The important point is that the modeled near-uniaxial tensile stress regime is consistent with the observations, as the observed sense of slip will result when a pre-existing fault is subjected to a tensile stress.

A comparison of Figs. 6a and 7a shows that ridge-parallel compressive stresses modeled at the Gorda ridge are not represented in the data. Whether the observations are indicative of the stress field in the plate or at the plate boundary is uncertain. We consequently cannot take these observations to accept or reject the model. In the Gorda interior, model stresses are within the uncertainty of observed stress directions but they systematically deviate. Model stresses in the Gorda region may be incorrect due to forces which were not taken into account. For instance, Furlong and Govers [48] invoked drag forces acting on the Juan de Fuca plate to explain crustal thickening and gravity data in the Mendocino Triple Junction region. Alternatively, the adopted force parameterization may be too simple as the model results are based on uniform values of resistive forces. Another cause of discrepancies may be if seismicity in the Gorda region occurs by fault reactivation. It is conceivable that these pre-existing

faults are systematically misoriented with respect to the current direction of maximum shear stress. The aim of this paper is to study the first order dynamics of the Juan de Fuca plate. As the stresses we compute agree with the observations to within the observation uncertainty, we defer from creating more complicated models to remove systematic orientation differences in the Gorda region.

Fig. 7b shows a detail of the stress model in Fig. 7a near the Nootka fault zone. Fig. 7c shows the result of introducing a fault into the mechanical model which represents the Nootka fault zone. Dynamically, this is a consistent procedure because the discontinuity does not introduce additional torques on the model. We impose a finite amount of friction on the model Nootka fault. Slip on the fault is a dynamic response to the force boundary conditions shown in Fig. 5a. Left lateral shear on the fault is visible in Fig. 7c from the offset of the mesh across the fault. This sense of shear agrees with what has been observed [3]. Overall, it is clear that deviatoric stress directions hardly change. Only in the immediate vicinity of the model fault are principal stress directions affected. As a consequence, the fit to observed stress directions does not improve or deteriorate.

Stress fields following from the set of force models where the eastern Explorer region is assumed to be a collision boundary are similar to those shown in Figs. 6 and 7. Our stress models at the scale of the whole Juan de Fuca plate are insensitive to the nature of this plate boundary section.

No observations directly constrain the average stress magnitude in the Juan de Fuca lithosphere. As a consequence we cannot discriminate between models with slabs penetrating to 200 km or 400 km, or between models with driving or resistive basal shear stresses.

We cannot resolve from our modeling whether the Pacific plate exerts a net transform push on the Juan de Fuca plate or not. Stress models for the transform push model and the no transform push model are virtually identical. Our results therefore provide no basis for considering transform push a relevant driving force in dynamic models of other plates. This is contrary to the conclusions of Wang et al. [7].

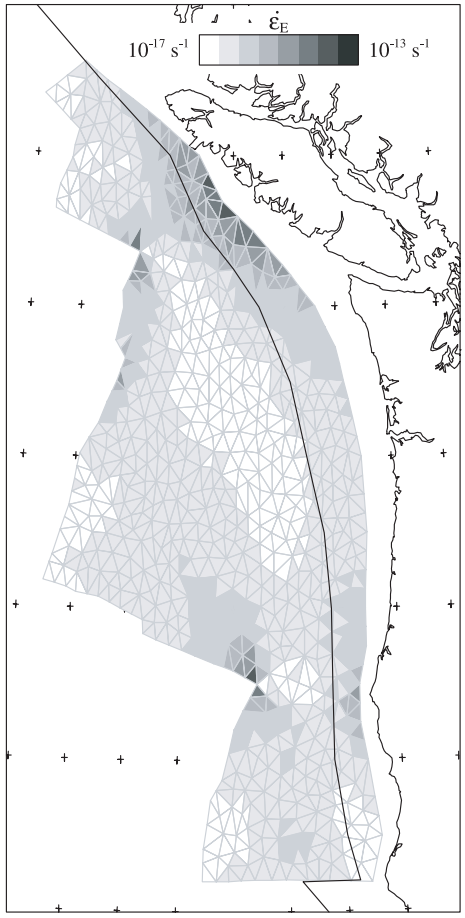

Fig. 8. Effective strain rates $\dot{\varepsilon}_E \equiv \sqrt{\dot{\varepsilon}_{ij}\dot{\varepsilon}_{ij}}$ computed from viscous relaxation during 1000 years of stresses of the 'transform push' model (Fig. 6a). Viscosities are assumed to depend on lithosphere age.

4.3. Rates of deformation in the Juan de Fuca plate

Seismicity and fault offset data are indicative of strain rate magnitudes. These observations can be compared with model results once we define how stresses in a lithosphere column cause deformation of that column. In other words, we need to specify a rheology which is representative of the entire column. As we do not have quantitative observations of strain rates in the Juan de Fuca

region we focus on relative variations only. For this purpose it suffices to approximate the mechanical strength of a lithospheric column. We note that the Juan de Fuca plate is a relatively young oceanic plate, and the viscosity of its upper mantle will dominate the rate at which the plate deforms. We assume that power law creep controls the rate of deformation in the upper mantle. We use experimental parameters from Kirby [49] for dry olivine. The temperature (or age) dependence of viscosity is accounted for by computing the temperature at 6 km depth using the GDH1 model [39].

Strain rates are calculated by solving Eq. 2 using a elastic-viscous rheology and integrating for a period of 1000 years. This is short on geologic time scales and the resulting strain rates, shown in Fig. 8, could be considered as the instantaneous response of the model to the stresses in Fig. 6a. The main part of the central Juan de Fuca plate deforms relatively slowly. The Nootka fault zone shows up in the model as a continuous band of relatively high strain rates. This is different in the northern Gorda region, where isolated strain rate highs are separated by a zone of little deformation. This may explain why the Explorer region is currently fragmenting from the Juan de Fuca plate and why the Gorda region is not. These contrasting responses to similar stresses are primarily caused by differences in lithospheric age.

Model strain rate magnitudes are not expected to have a one-to-one correspondence with seismicity, because some of the deformation may be occurring aseismically and because the seismic catalog of the region is short. Therefore, high model strain rates do not necessarily coincide with high seismicity. Low model strain rates should be indicative of low seismicity. In general, the match between strain rate magnitudes and seismicity (Fig. 1a) is not good. Observations and model results are compatible in the aseismic central Juan de Fuca plate. The model fails to reproduce the NW–SE striking seismicity band in the Gorda region. This can be explained by the fact that deformation in the Gorda region has been observed to occur along bathymetric discontinuities, probably faults [5]. As discussed in Section 4.2, faults in this region may also cause a systematic misorientation of modeled and observed stress directions. Our simple viscous model does not account for this type of deformation. The SSE–NNW striking seismicity band in the Explorer region is also not predicted by the model. Most of the Explorer region is probably younger than 2 Myr, and therefore more susceptible to relatively small variations in the boundary forces acting on the region. These variations cannot be resolved in the present study on the dynamics of the complete Juan de Fuca plate, and will be the topic of a more detailed modeling study of deformation in the Explorer region (Govers, Furlong and Rohr, manuscript in preparation). Strain rates are also predicted to be relatively high off Endeavour ridge. This is the region which was selected by the ODP Leg 168 Scientific Party to investigate hydrothermal processes because the sediments were completely undisturbed. However, deformation in our model occurs in a direction perpendicular to the studied section (Figs. 1a and 6), which is why it does not need to show up in the seismics. In addition, model strain rates are high near the ridge, where no sediment cover was found. Beyond the point where sediments were seen in the seismics, model strain rate magnitudes are several orders of magnitude lower.

5. Conclusions

Typical plate forces like slab pull, ridge push, transform shear resistance and subduction resistive forces are combined with a new type of driving force, transform push, to establish a dynamic model for the present-day Juan de Fuca plate. Transform push would result from normal stresses transmitted across transform faults and the Mendocino Transform fault has been proposed to be subject to transform push. Various force models result from the constraint that net torque on the Juan de Fuca plate vanishes. The models can be divided into a group of models which do require transform push, and a group of models which do not require transform push.

Intraplate stresses resulting from the force models are identical in terms of principal stress directions – they do differ in stress magnitudes. As

there are no observations which constrain lithospheric stress magnitudes, we cannot discriminate between the various force models.

The mechanism which primarily causes intraplate stresses in the Juan de Fuca plate is very similar to that for the Farallon plate before it broke into the Nazca and Cocos plates [6]. Relatively young ages at the trench in the Explorer and Gorda regions cause net resistance to the net pull at the trench in the central region (Fig. 6, inset). The resulting in-plane bending of the plate causes trench-parallel tension in the east and roughly N–S compression in the west. Stress models are insensitive to whether the Explorer–North America plate boundary is a collision or a subduction plate boundary. The fit of model deviatoric stress directions and stress indicators is acceptable. We therefore conclude that the stress model is correct to first order.

Model stresses around the Nootka fault zone and the northern Gorda region are similar. Therefore, we propose that differences in lithosphere age in these regions are primarily responsible for differences in the mechanical properties in these regions. As a consequence, the Explorer region is severing from the Juan de Fuca plate and the Gorda region is not.

Differences between stress models with and without transform push are negligible. We therefore conclude that Juan de Fuca dynamics do not require the introduction of this new plate driving force in plate force models.

Acknowledgements

Stijn Teeuwisse calculated preliminary force and stress models which formed the basis of this paper. We thank Doug Wilson of the Department of Geological Sciences of the University of California at Santa Barbara for determining ages of the shallow subducted slab and for providing us electronic versions of his Juan de Fuca age data. Jay Melosh of the Lunar and Planetary Lab and Department of Geosciences in Tucson, AZ, is gratefully acknowledged for sharing his mechanical finite element code. We thank David Coblentz and Scott King for their reviews. R.G. was partially supported by NATO Grant CRG.960139. This work was conducted under the program of the Vening Meinesz Research School of Geodynamics. *[SK]*

References

[1] T. Atwater, Plate tectonic history of the northeast Pacific and western North America, in: E.L. Winterer, D.M. Hussong, R.W. Decker (Eds.), The Eastern Pacific Ocean and Hawaii. The Geology of North America N, Geological Society of America, 1989, pp. 21–72.

[2] P. Lonsdale, Structural patterns of the Pacific floor offshore of peninsular California, in: J.P. Dauphin, B.R.T. Simoneit (Eds.), The Gulf and Peninsular Province of the Californias, AAPG Mem. 47 (1991) 87–124.

[3] R.D. Hyndman, R.P. Riddihough, R. Herzer, The Nootka fault zone – a new plate boundary off western Canada, Geophys. J. R. Astron. Soc. 58 (1979) 667–683.

[4] D.S. Wilson, Confidence intervals for motion and deformation of the Juan de Fuca plate, J. Geophys. Res. 88 (1993) 16,053–16,071.

[5] D.S. Wilson, Deformation of the so-called Gorda plate, J. Geophys. Res. 94 (1989) 3065–3075.

[6] R. Wortel, S. Cloetingh, On the origin of the Cocos-Nazca spreading center, Geology 9 (1981) 425–430.

[7] K. Wang, J. He, E.E. Davis, Transform push, oblique subduction resistance, and intraplate stress of the Juan de Fuca plate, J. Geophys. Res. 102 (1997) 661–674.

[8] W. Spence, Stress origins and earthquake potentials in Cascadia, J. Geophys. Res. 94 (1989) 3076–3088.

[9] R.P. Denlinger, A model for large-scale plastic yielding of the Gorda deformation zone, J. Geophys. Res. 97 (1992) 15,415–15,423.

[10] C.G. Fox, W.E. Radford, R.P. Dziak, T.-K. Lau, H. Matsumoto, A.E. Schreiner, Acoustic detection of a seafloor spreading episode on the Juan de Fuca Ridge using military hydrophone arrays, Geophys. Res. Lett. 22 (1995) 131–134.

[11] R. Wahlström, G.C. Rogers, Relocations of earthquakes west of Vancouver Island, British Columbia, 1965–1983, Can. J. Earth Sci. 29 (1992) 953–961.

[12] D.P. McKenzie, The relation between fault plane solutions for earthquakes and the directions of the principal stresses, Bull. Seismol. Soc. Am. 59 (1969) 591–601.

[13] C. Goldfinger, L.D. Kulm, R.S. Yeats, L.C. McNeill, C. Hummon, Oblique strike-slip faulting of the central Cascadia submarine forearc, J. Geophys. Res. 102 (1997) 8217–8243.

[14] E.E. Davis, M.J. Mottl, A.T. Fisher et al., Proc. ODP Init. Reports 139, Ocean Drilling Program, College Station, TX, 1992.

[15] E.E. Davis, H. Villinger, Tectonic and thermal structure of the Middle Valley sedimented rift, northern Juan de Fuca ridge, in: E.E. Davis, M.J. Mottl, A.T. Fisher et

al. (Eds.), Proc. ODP Init. Reports 139, Ocean Drilling Program, College Station, TX, 1992, pp. 9–41.
[16] E.E. Davis, A.T. Fisher, J.V. Firth et al., Proc. ODP Init. Reports 168, Ocean Drilling Program, College Station, TX, 1997.
[17] K.M.M. Rohr, Increase of seismic velocities in upper oceanic crust and hydrothermal circulation in the Juan de Fuca plate, Geophys. Res. Lett. 21 (1994) 2163–2166.
[18] B. Müller, V. Wehrle, K. Fuchs, The 1997 release of the World Stress Map (available on-line at http://www-wsm.physik.uni-karlsruhe.de/pub/Rel97/wsm97.html) 1997.
[19] R.M. Richardson, Finite element modeling of stress in the Nazca plate: driving forces and plate boundary elements, Tectonophysics 50 (1978) 223–248.
[20] S. Cloetingh, R. Wortel, Stress in the Indo-Australian plate, Tectonophysics 132 (1986) 49–67.
[21] D.D. Coblentz, S. Zhou, R.R. Hillis, R.M. Richardson, M. Sandiford, Topography, boundary forces, and the Indo-Australian intraplate stress field, J. Geophys. Res. 103 (1998) 919–931.
[22] R.M. Richardson, L.M. Reding, North America plate dynamics, J. Geophys. Res. 96 (1991) 12,201–12,223.
[23] M.J.R. Wortel, M.J.N. Remkes, R. Govers, S.A.P.L. Cloetingh, P.Th. Meijer, Dynamics of the lithosphere and the intraplate stress field, Phil. Trans. R. Soc. London A 337 (1991) 111–126.
[24] P.Th. Meijer, M.J.R. Wortel, The dynamics of motion of the South American plate, J. Geophys. Res. 97 (1992) 11,915–11,931.
[25] M. Stefanick, D.M. Jurdy, Stress observations and driving force models for the South America Plate, J. Geophys. Res. 97 (1992) 11,905–11,913.
[26] D.D. Coblentz, R.M. Richardson, Analysis of the South American intraplate stress field, J. Geophys. Res. 101 (1996) 8643–8657.
[27] P.Th. Meijer, R. Govers, M.J.R. Wortel, Forces controlling the present-day state of stress in the Andes, Earth Planet. Sci. Lett. 148 (1997) 157–170.
[28] D.D. Coblentz, M. Sandiford, Tectonic stresses in the African plate: Constraints on the ambient lithospheric stress state, Geology 22 (1994) 831–834.
[29] P.Th. Meijer, M.J.R. Wortel, Cenozoic dynamics of the African plate with emphasis on the Africa-Eurasia collision, J. Geophys. Res. 104 (1999) 7405–7418.
[30] D.W. Forsyth, S. Uyeda, On the relative importance of the driving forces of plate motion, Geophys. J. R. Astron. Soc. 43 (1975) 163–200.
[31] R. Govers, M.J.R. Wortel, S.A.P.L. Cloetingh, C.A. Stein, Stress magnitude estimates from earthquakes in oceanic plate interiors, J. Geophys. Res. 97 (1992) 11,749–11,759.
[32] Bathymetric map of the continental margin of western Canada, 2/e, Pacific Geoscience Centre, Earth Physics Branch, Ottawa, ON, 1985.
[33] A.M. Trehu, I. Asudeh, T.M. Brocher, J. Luetgert, W.D. Mooney, J.L. Nabelek, Y. Nakamura, Crustal architecture of the Cascadia forarc, Science 266 (1994) 237–243.
[34] R. Riddihough, R.D. Hyndman, Queen Charlotte Islands margin, in: E.L. Winterer, D.M. Hussong, R.W. Decker (Eds.), The Eastern Pacific Ocean and Hawaii. The Geology of North America N, Geological Society of America, 1989, pp. 403–411.
[35] K.M.M. Rohr, K.P. Furlong, Ephemeral plate tectonics at the Queen Charlotte triple junction, Geology 23 (1995) 1035–1038.
[36] C. Kreemer, R. Govers, K.P. Furlong, W.E. Holt, Plate boundary deformation between the Pacific and North America in the Explorer region, Tectonophysics 293 (1998) 225–238.
[37] D.S. Cowan, M. Botros, H.P. Johnson, Bookshelf tectonics: Rotated crustal blocks within the Sovanco Fracture Zone, Geophys. Res. Lett. 13 (1986) 995–998.
[38] C.R.B. Lister, Gravitational drive on oceanic plates caused by thermal contraction, Nature 257 (1975) 663–665.
[39] C.A. Stein, S. Stein, A model for the global variation in oceanic depth and heat flow with lithospheric age, Nature 359 (1992) 123–129.
[40] R.D. Müller, W.R. Roest, J.-Y. Royer, L.M. Gahagan, J.G. Sclater, Digital isochrons of the world's ocean floor, J. Geophys. Res. 102 (1997) 3211–3214.
[41] E.D. Humphreys, K.G. Dueker, Western US mantle structure, J. Geophys. Res. 99 (1994) 9615–9634.
[42] H. Bijwaard, W. Spakman, E.R. Engdahl, Closing the gap between regional and global travel time tomography, J. Geophys. Res. 103 (1998) 30,055–30,078.
[43] D.S. Wilson, Tectonic history of the Juan de Fuca ridge over the last 40 million years, J. Geophys. Res. 93 (1988) 11,863–11,876.
[44] J. van den Beukel, Thermal and mechanical modelling of convergent plate margins, Geol. Ultraiect. 62 (1990) 126 pp.
[45] P. England, R. Wortel, Some consequences of the subduction of young slabs, Earth Planet. Sci. Lett. 47 (1980) 403–415.
[46] M.J.R. Wortel, S.A.P.L. Cloetingh, Accretion and lateral variations in tectonic structure along the Peru-Chile Trench, Tectonophysics 112 (1985) 443–462.
[47] H.J. Melosh, A. Raefsky, The dynamical origin of subduction zone topography, Geophys. J. R. Astron. Soc. 60 (1980) 333–354.
[48] K.P. Furlong, R. Govers, Ephemeral crustal thickening at a triple junction: The Mendocino crustal conveyor, Geology 27 (1999) 127–130.
[49] S.H. Kirby, Rheology of the lithosphere, Rev. Geophys. Space Phys. 21 (1983) 1458–1487.
[50] C. DeMets, R.G. Gordon, D.F. Argus, S. Stein, Effect of recent revisions to the geomagnetic reversal time scale on estimates of current plate motions, Geophys. Res. Lett. 21 (1994) 2191–2194.